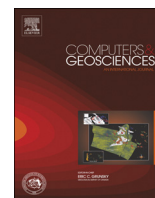




ELSEVIER

Contents lists available at ScienceDirect

Computers & Geosciences

journal homepage: www.elsevier.com/locate/cageo

Using Kinect to analyze pebble to block-sized clasts in sedimentology

G. Moreno Chávez^{a,*}, D. Sarocchi^{b,1}, E. Arce Santana^{c,2}, L. Borselli^b,
L.A. Rodríguez-Sedano^{d,3}^a Doctorado Institucional en Ingeniería y Ciencias de Materiales, c/o Instituto de Geología UASLP, Av. Dr. M. Nava No 5, Zona Universitaria, 78290 San Luis Potosí, Mexico^b Instituto de Geología/Fac. de Ingeniería UASLP, Av. Dr. M. Nava No 5, Zona Universitaria, 78290 San Luis Potosí, Mexico^c Facultad de Ciencias, UASLP, Diagonal Sur S/N, Zona Universitaria, 78290 San Luis Potosí, Mexico^d Posgrado Centro de Geociencias, UNAM, Blvd. Juriquilla No. 3001, 76230 Querétaro, Mexico

ARTICLE INFO

Article history:

Received 18 February 2014

Received in revised form

3 July 2014

Accepted 4 July 2014

Available online 14 July 2014

Keywords:

Kinect device

Depth measurement

Optical granulometry

Fourier transform

Level sets

ABSTRACT

In this paper, we propose a new system for automatically measuring grain sizes in a range from pebbles to blocks. The system is based on use of the Microsoft Kinect device and a novel software developed by the authors which enables a tridimensional digital model of a selected area of an outcrop to be captured. With the tridimensional model, clasts are stacked using new segmentation algorithms based on level sets and Fourier analysis. The resulting binary image (clasts and matrix) is analyzed by means of the Rosiwal stereological method. The granulometric Cumulative Distribution Function (CDF), obtained automatically by this new methodology, was compared to the granulometric CDF, obtained manually by the Rosiwal technique, by means of a Kolmogorov–Smirnov test. The comparison showed good agreement between the methods and demonstrated that this inexpensive system (already used in several scientific fields) with great potential can also be used to obtain fast, automatic and accurate grain size distributions of sedimentary deposits. The software tools used to control the Kinect device, which provide the three-dimensional elevation models of the outcrops and allows its analysis, are freely available from the author.

© 2014 Elsevier Ltd. All rights reserved.

1. Introduction

Granulometry is an essential tool for the study of sedimentary deposits. Particle size distribution is directly related to the origin, transport and deposition of the particulate materials that constitute a deposit. The statistical study of granulometric distributions reveals key indicators of sedimentary texture and structures which would not be as evident or even impossible to observe by naked eye such as gradation, coarse or finer particles lenses and sedimentary structures (Sarocchi et al., 2005). A study of vertical and longitudinal changes in granulometry along a deposit enables transport and deposition mechanisms to be inferred. Saucedo

et al. (2008) and Sarocchi et al. (2011) used this analysis in debris flow and block-and-ash flow deposits.

Granulometric studies are performed by means of different analytical techniques such as image analysis, sieving and laser diffraction (Syvitski, 1991; Sarocchi et al., 2011), because of the wide range of particle sizes contained in the sedimentary deposits. Some sedimentary deposits are so poorly sorted that they may contain particles from a few microns to several meters in size. An analytical method widely used since the early days of sedimentology has been sieving, and until recent decades it was the only method used for granulometric studies (Allan, 2003; Bunte and Abt, 2001). Sieving enables measurement of particles in the range between -5 and $+5$ phi (32 mm to 0.031 cm); however, if only sieving is used on poor sorted deposits such as pyroclastic and debris flows, debris avalanche or olistostromes (Olgun and Norman, 1993; Saucedo et al., 2008; Roverato et al., 2011; Sarocchi et al., 2011), between others, much of the important information contained in the coarse and fine tails of the distribution is lost. For this reason it becomes necessary to use sieving in conjunction with other analytical methods to also enable the analysis of particles in the fine and coarse distribution tails (Saucedo et al., 2008; Sarocchi et al., 2011). Fine particles are commonly analyzed

* Corresponding author. Tel.: +52 444 817 1039; fax: +52 444 811 1741.

E-mail addresses: gamalielmch@gmail.com (G. Moreno Chávez), sarocchi@gmail.com (D. Sarocchi), arce@fciencias.uaslp.mx (E. Arce Santana), lborselli@gmail.com (L. Borselli), lrodriguez2021@live.com.mx (L.A. Rodríguez-Sedano).¹ Tel.: +52 444 8171039; fax: +52 444 811 1741.² Tel.: +52 444 8262316.³ Tel.: +52 442 238 1104.

by means of photo-sedimentation or stream scanning methods (Stein, 1985; Lovell and Rose, 1991; Lewis and McConchie, 1994) while the coarser particles are analyzed by means of optical granulometry techniques based on image analysis (Sahagian and Proussevitch, 1998; Sarocchi et al., 2005, 2011; Jutzeler et al., 2012).

Optical granulometry techniques consist in taking pictures of the outcrops with a scale reference superimposed, segmenting the particles (generally with methods based on grayscale or color selection) and selecting the area of interest to obtain a binary image of the particles to be analyzed. A stereological method (Mouton, 2002; Sahagian and Proussevitch, 1998; Sarocchi et al., 2005, 2011; Jutzeler et al., 2012) is then applied to obtain the volumetric particle size distribution. However, images of natural geological deposits are rarely easy to segment due to the low contrast in gray tones and colors between different granulometric components. For this reason algorithms with smarter and more efficient segmentation criteria are required because the only alternative to optical granulometric analysis is a lengthy, tedious semi-manual method (Sarocchi et al., 2005, 2011).

In many cases, useful information for segmenting large clasts from sedimentary deposits can be derived from 3D scans of the clasts protruding from the base level of a Digital Elevation Model (DEM). In this paper we propose a new optical method which is based on the use of a DEM of outcrops obtained by means of a Microsoft Kinect device. The equipment utilized is an Xbox 360™ console accessory, with moderate spatial (2–20 mm) and depth resolution (1–75 mm), working in real time (30 fps). The equipment is inexpensive, small in size, lightweight, and can be used

with a simple laptop equipped with an USB port. Kinect applications are growing in diverse scientific and educational areas such as computational graphics, image processing, computational vision, and human-machine interfaces (Cruz et al., 2012; Liying et al., 2012). Mankoff and Russo (2012) demonstrated that this device can be usefully employed in many earth science disciplines.

We propose the use of the Kinect for automatic analysis of coarse clasts (pebbles to blocks) as a complement to data obtained using other methods for a complete granulometric analysis of sedimentary deposits. Specific software has been developed to manage the device, capture color images and construct a DEM of the outcrop, perform image segmentation (which is based on level



Fig. 1. Kinect device.

Table 1
Infrared camera area and resolution with respect to distance.

Kinect–plane distance (m)	Area (m ²)	Depth resolution (mm)
0.5	~0.7	1
1	~1.4	3
5	~7	75

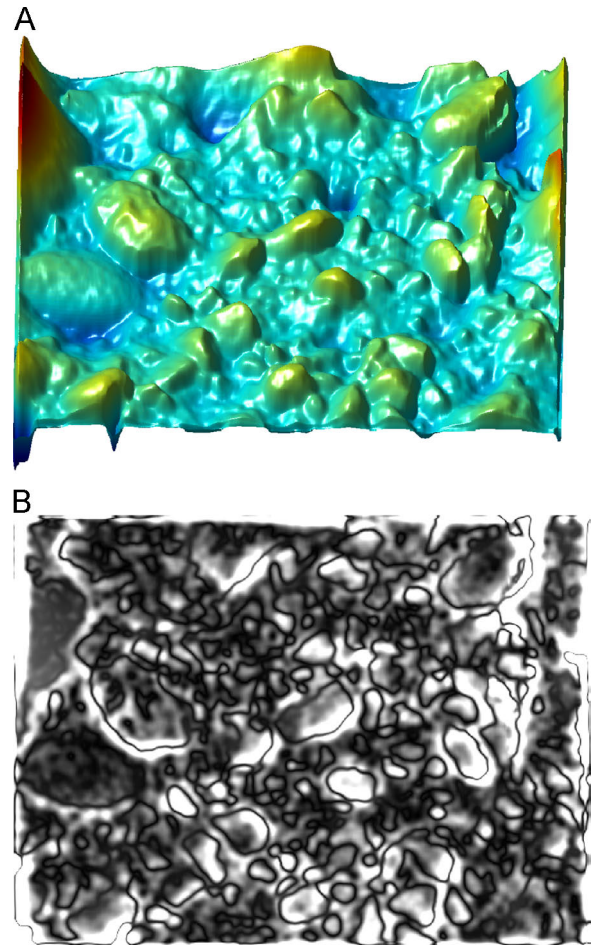


Fig. 3. (A) The depth image of area 4 and (B) its filtering by a Gaussian low-pass filter in the frequency domain.

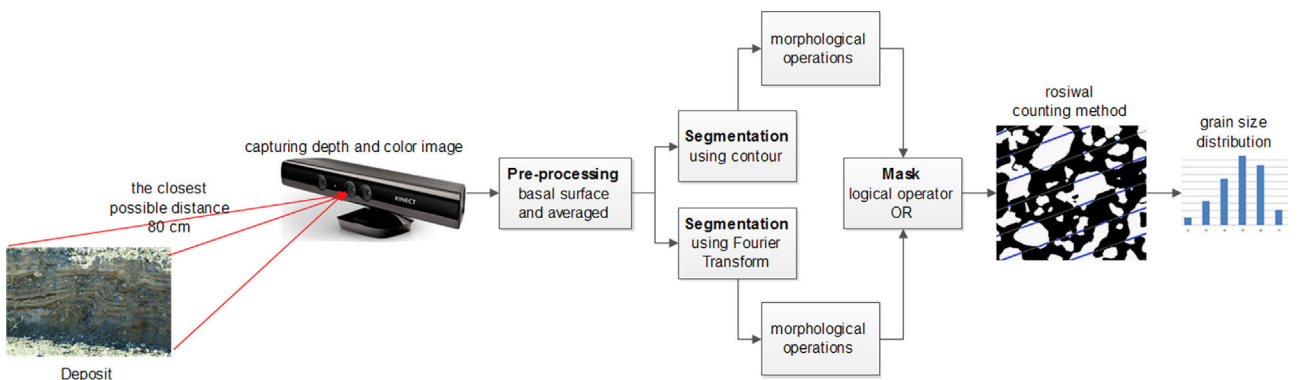


Fig. 2. Schematic diagram of the capture of the DEM of the outcrop, DEM processing and Rosiwal analysis.

sets and 2D Fourier analysis), and carry out optical granulometry analysis using Rosiwal's stereologic method (Chayes, 1956; Sarocchi et al., 2005, 2011). The software presented here is original and freely distributed.

The method has been tested on four different sedimentary and volcano-sedimentary deposits. The first deposit is a quaternary conglomerate located near the city of San Luis Potosí, Mexico. Five different areas of the same outcrop were analyzed. The second deposit is an alluvial deposit outcropping in a ravine close to the Joya Honda maar, a 0.6 My old volcano, forty kilometers north of the city of San Luis Potosí, Mexico. The third outcrop is a lahar deposit in the north flank of the Quaternary Nevado de Toluca volcano, Toluca, Mexico. The last outcrop belongs to the Joya Honda pyroclastic deposit, whose origin is related to hydromagmatic explosions.

Both the Kinect 3D automatic method and the optical semi-manual Rosiwal's intercepts method were applied to obtain the granulometric distribution (Sarocchi et al., 2005, 2011) of these four deposits. The results show very good agreement between the Kinect 3D method and the semi-manual Rosiwal method, confirming the potential usefulness of the automatic analysis performed using the Kinect device and original software. The currently moderate resolution of the Kinect limits the application of the method to the analysis of coarse clasts and makes it necessary to combine the information with data obtained by sieving and photosedimentographic methods. However, development of specific software will significantly improve the resolution of DEMs that can be obtained with this Kinect model. Moreover, Microsoft has announced future releases of new devices with

sensors providing better depth, spatial and detail resolution, so it seems likely that in the near future these systems could be better tools for measuring particle size geology.

2. Kinect device

The Microsoft Kinect was developed by PrimeSense and Microsoft Game Studio, and it was first released on November 4, 2010, as an accessory for the Xbox 360™ videogame console. But it was not until December 9 that PrimeSense Co. released the driver and framework API- Open Natural Interaction (OpenNI) codes for public access. The Microsoft Kinect has a depth sensor, RGB camera, accelerometer, motor and a series of microphones. A photograph of the Kinect device is shown in Fig. 1.

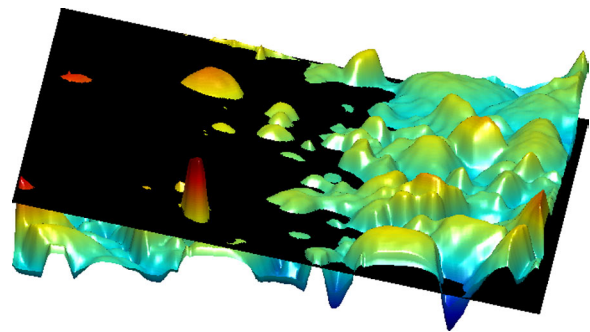


Fig. 5. Intersection of an inclined plane with an area of the outcrop.

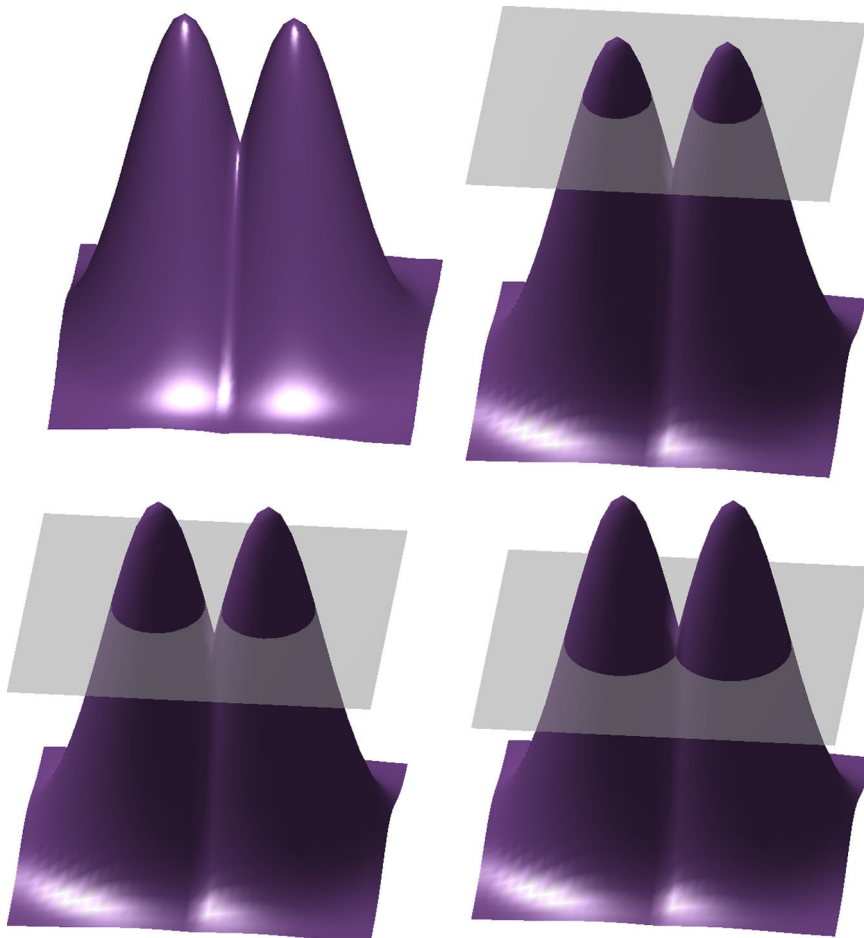


Fig. 4. Illustration of the level sets algorithm.

2.1. Depth sensor

The depth measuring system has an infrared laser emitter and an infrared camera. The emitter projects a known pattern of points which undergoes deformation as a function of depth. The infrared camera captures the deformed pattern of points and the depth is calculated based on the difference between the emitted pattern

and the captured pattern. The distance between the emitter and the camera is 7.5 cm. A fundamental feature for an accurate measurement is calibration between the projector and the infrared camera, because it can be altered by many factors (Cruz et al., 2012; Jingjing et al., 2012; Zhengyou, 2012). We consider depth measurement as a geometric characteristic of the scene.

The infrared camera shoots 30 frames per second (fps) with a resolution of 1200×960 pixel, but in order to make USB transmission more efficient, the image is subsampled at a resolution of 640×480 at 11 bit. The field of vision (FOV) is 58 horizontal, 45 vertical and 70 diagonal degrees. The focal length is 6.1 mm. The recommended range of depth is from 0.8 to 3.5 m, although in Mankoff and Russo (2012) they present measures up to 5 m with an error of 1% in controlled conditions. The area of the FOV depends on the distance between the Kinect and the plane; the less the distance, the smaller the area, and vice versa. The background resolution decreases with distance, as documented by Khoshelham and Elberink (2012), who conclude that it decreases by a quadratic factor in controlled conditions, and by Mankoff and Russo (2012) who reported that accuracy is 1 mm at a distance of

Table 2
Geometric characteristics of shots.

Outcrop	Kinect—outcrop distance [cm]	Calculated area [m ²]
Area 1	103	1.0626
Area 2	86	0.6894
Area 3	89	0.7400
Area 4	94	0.8152
Area 5	85	0.6804
Area 6	87	0.6963
Area 7	89	0.7400
Area 8	88	0.7115

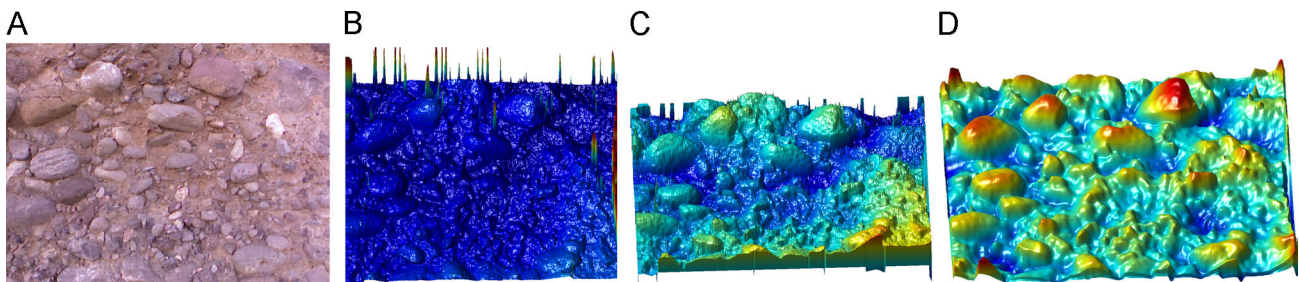


Fig. 6. Preprocessing. (A) Color image of area 1; (B) depth image captured; (C) arithmetic mean of depth image; (D) processed Gaussian kernel filter of C. (For interpretation of the references to color in this figure legend, the reader is referred to the web version of this article.)

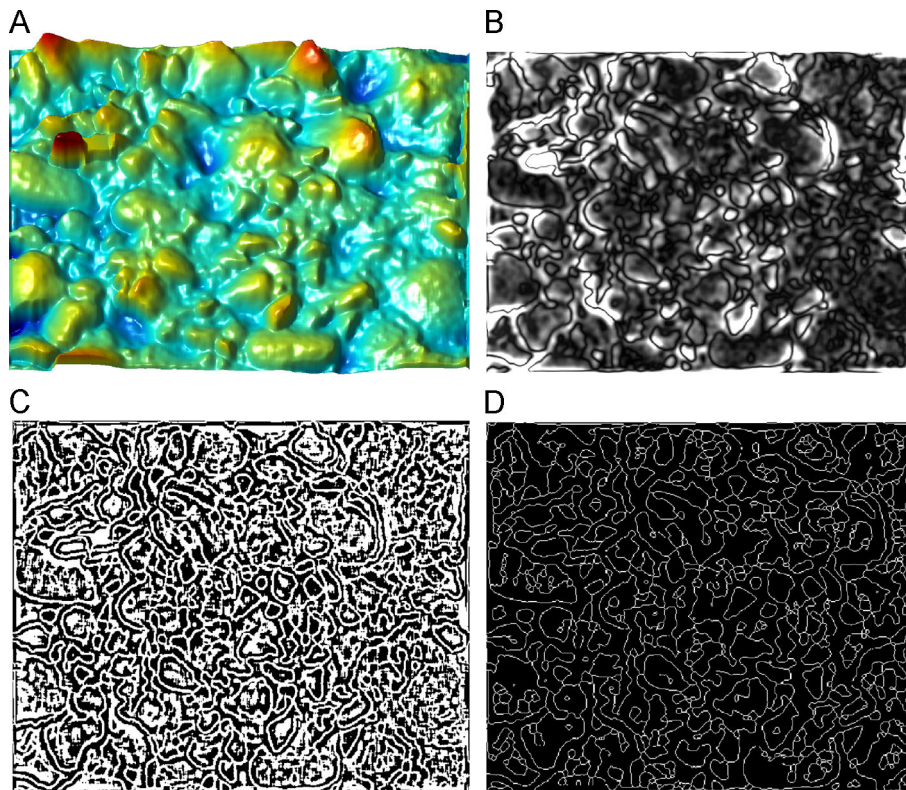


Fig. 7. Segmentation algorithm based on Fourier and morphological operations. In (A) preprocessed depth image, (B) results of Fourier Transform and filtered Gaussian low pass, (C) image generated by LoG filter and converted to binary image by threshold equal to 0.05, (D) image resulting from clean, spur and thin morphological operations.

0.5 m and 75 mm at 5 m. Table 1 shows the FOV area and its depth resolution at various distances; these data were obtained by Mankoff and Russo (2012). Smisek et al. (2011) present an equation giving the resolution as a function of distance that resulted from fitting a polynomial curve to measurements at distances between 0.5 and 5 m:

$$q(z) = 2.73z^2 + 0.75z - 0.58 \quad (\text{mm}) \quad (1)$$

where q is the resolution and z the distance in meters.

2.2. Color camera

The color camera has a FOV of 63° horizontally and 50° vertically with a focal length of 2.9 mm. It works at two frequencies depending on the desired resolution. For a resolution of 1280×1024 it works at 10 fps, and for VGA resolution (640×480), at 30 fps, both at 8 bit per channel. The image color formats may be RGB or YUV (Islam et al., 2013). An important characteristic of this device is that it is possible to capture the color image and the depth image at the same time. In this way we have two images from the same scene, one representing its elevation and the other its color, and these two images can easily be aligned.

2.3. Accelerometer, motor and microphones

The accelerometer and the motor enable the Kinect to take a position on the axis at a varying angle between -27° and 27° , and it can auto-adjust within this range to the desired angle independently of the base position of the device. The four-microphone array of the Kinect samples at a frequency of 16 kHz per channel and is used to determine the direction of the sound.

2.4. Software

There are open libraries available mainly on three platforms. OpenKinect is a community of libraries and projects of released code based mainly on the libfreenect driver that can operate in Windows, Linux and Mac (OpenKinect, 2013). OpenNI is a multi-language cross-platform framework, with libraries and applications for 3D structures (OpenNI, 2013). Microsoft Kinect for Windows has created C language applications, Visual Basic and an interface Developer Toolkit (Windows, 2013).

2.5. Sources error and limitations

The error sources using the Kinect are mainly related to three aspects: the measurement setup, sensor errors and properties of the objects. Perhaps one of the most important is lighting conditions because this diminishes the contrast of infrared image points, which can cause an error in depth calculation or holes in the depth map. Another problem is the angle and the distance between the surface and the Kinect. Protruding objects can produce shadows on the depth map, depending on the angle between the infrared emitter and the surface. The bigger the height and area of the objects, the larger the error obtained. A way to avoid this error is placing the device perpendicular to the plane. The second source of error is related to sensor errors because the depth measurement is based on the distance between the infrared projector and the camera. Inaccurate readings from these sensors caused by shock or vibration may produce an inaccurate depth map. Finally, the optical properties of objects such as translucency or diffuse reflection produce holes in the depth map (Essmaeel et al., 2012; Khoshelham and Elberink, 2012; Jungong et al., 2013).

3. Materials and methods

In this section the main characteristics of the outcrops and the initial instrumental setup for field work are described. The methodology is divided into three sections: the first step is to obtain the DEM of the outcrop. Then the segmentation is performed using the level sets algorithm and bidimensional transformed Fourier analysis. When the segmentation is ready, the morphologic operations are performed, and the last step consists in carrying out the count analysis by Rosiwal's intercept method.

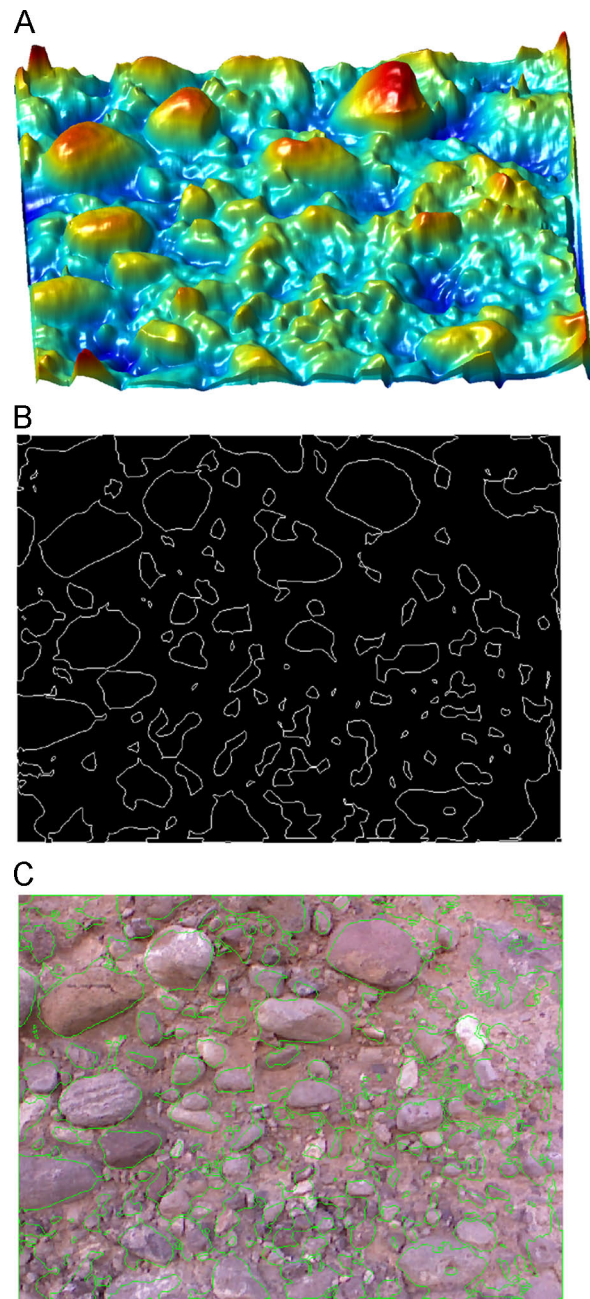


Fig. 8. (A) Depth image corresponding to Area 1, (B) result of segmentation by level sets and (C) boundaries of the computing final mask shown in green. (For interpretation of the references to color in this figure legend, the reader is referred to the web version of this article.)

3.1. Kinect and outdoor experimental setup

Eight areas of four different outcrops were analyzed using this methodology. Five areas (Area 1 to Area 5) correspond to a Quaternary conglomerate located near the city of San Luis Potosí, Mexico (22°9' 26.06"N, 101°2' 12.13"W), an alluvial deposit (Area 6) situated in a ravine close to the Joya Honda maar (22°25' 12.55" N, 100° 45' 2.55" W), a debris flow (Area 7) located in the north flank of the Nevado de Toluca volcano, Toluca, Mexico (19° 7' 54.03" N, 99° 40' 58.08") and a pyroclastic deposit (Area 8) pertaining to the Joya Honda maar volcanic sequence (22° 25' 17.61" N, 100° 46' 58.67" W).

The outdoor analysis was conducted between 6:00 and 7:00 p. m. on July 2013 with a small amount of indirect natural light due to the limitations, mentioned above, of the infrared camera. We attempted to make distances between the Kinect and the outcrop as near as possible to 80 cm. At each of the eight areas one color image was taken, and 100 shots to measure the depth. The matrix coordinates of the correspondence between the color image and depth image were also recorded. In order to achieve the most stable image possible, the Kinect was mounted on a tripod with a base that allowed the Kinect to move 70 cm to the left and the right from the center position, and to slide vertically 80 cm from the bottom position. This setup is shown in Fig. 2. The power

source in the field was a 12 V 18.5 A car battery used in conjunction with a DC/AC power inverter.

3.2. Framework segmentation and pre-processing

This section presents the notation used and pre-processing operations. We call the image of the outcrop captured with the Kinect "depth image" and denote it by $I(r)$, where the vector $r = \{(x, y) | 1 < x < L_x, 1 < y < L_y\}$ represents the spatial position of the depth in the range $0m < I(r) < 5m$. We consider that the depth image $I(r)$, consisting of regions, is a set belonging to the classes $\{c_1, c_2, \dots, c_m\}$ where m is the number of sites that represent the area of the clasts and matrix. Each pixel r in the image is assigned a unique label $r \in \{c_1, c_2, \dots, c_m\}$, which depends on its height and spatial position.

The first pre-processing module produces the average of the captured images. This is $\bar{I}(r)$, the arithmetic mean of the 100 shots, defined as

$$\bar{I}(r) = \frac{\sum_{n=1}^{100} I_n(r)}{100} \tag{2}$$

To reduce the errors caused by potential artifacts introduced to the depth acquisition, mainly due to the edges of the object and

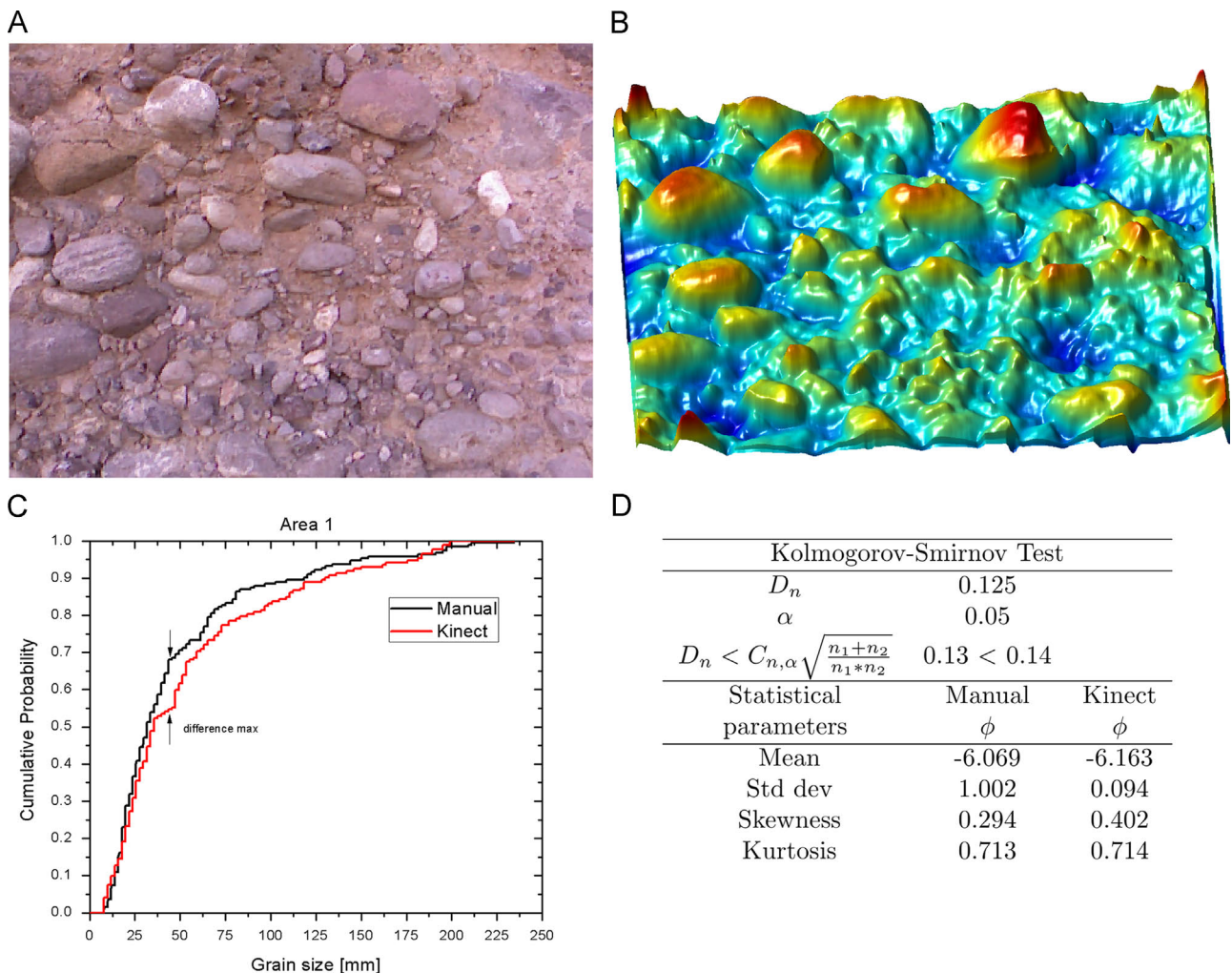


Fig. 9. Results obtained from Area 1, Quaternary conglomerate. (A) Color image; (B) depth image; (C) graph of ECDF resulting from manual analysis and automatic method, obtaining a maximum difference of 12.5%; and (D) Kolmogorov–Smirnov test and statistical parameters. (For interpretation of the references to color in this figure legend, the reader is referred to the web version of this article.)

the type of material, we set a threshold θ to apply to the depth image, which was fixed experimentally at three times the average of the depth data ($\forall \tilde{I}(r) > \theta, \hat{I}(r) = 0$) and $\hat{I}(r) = \tilde{I}(r)$ otherwise and smoothed this image by convolving $\hat{I}(r) = \tilde{I}(r) \times G_\sigma$ where G_σ is a Gaussian kernel filter with standard deviation σ . The filter formula is expressed as

$$G(x, y, \sigma) = \frac{1}{2\pi\sigma^2} \exp\left(-\frac{x^2 + y^2}{2\sigma^2}\right). \quad (3)$$

Now we assume the depth image to be a topographic surface, which can be represented as the sum of three components; a surface which belongs to the clasts, another corresponding to the outcrop matrix, and the envelope of the first two, which we call basal. This is expressed mathematically as $\hat{I}(r) = \hat{I}(r)_{clast} + \hat{I}(r)_{matrix} + \hat{I}(r)_{basal}$. To implement the segmentation algorithm proposed, we need that $\tilde{I}(r) = \hat{I}(r) - \hat{I}(r)_{basal}$ or, expressed in terms of the clasts and matrix surface, $\tilde{I}(r) = \hat{I}(r)_{clast} + \hat{I}(r)_{matrix}$. An approximation to the basal surface can be given by a polynomial whose coefficients are calculated using the regional minimum, which is a connectivity group such that the pixels of the group have the same value, with external pixels having higher values. To get a good approximation we carry out this process iteratively, so the basal

surface at iteration n is given by

$$\hat{I}(r)_{basal}^{(n)} = \hat{I}(r) - \sum_{m=1}^{n-1} \hat{I}(r)_{basal}^{(m)} \quad (4)$$

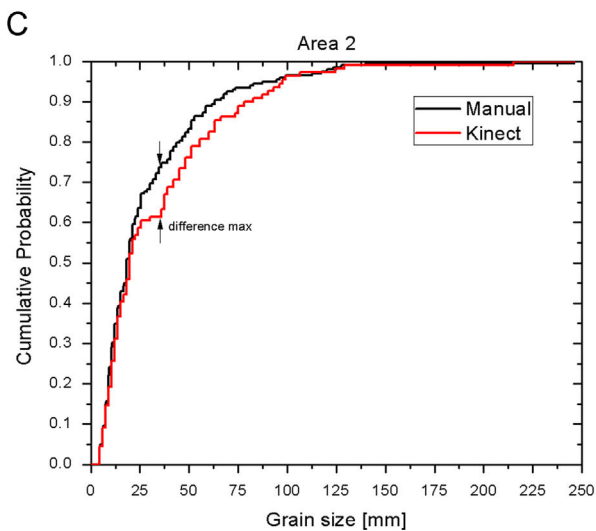
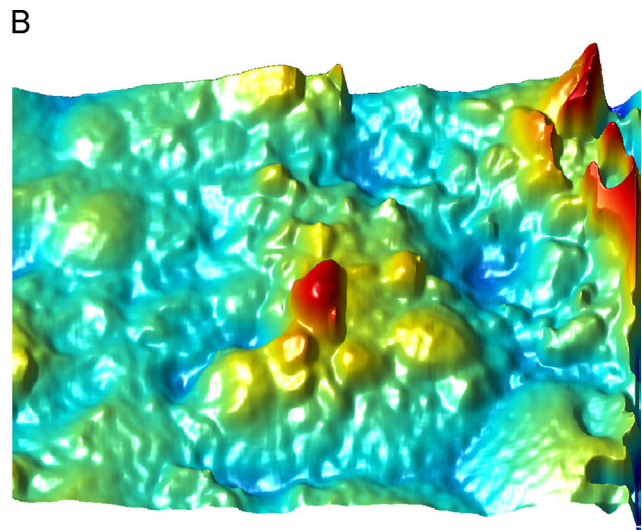
and the approximation to the total basal surface is given by

$$\hat{I}(r)_{basal} = \sum_{n=1}^N \hat{I}(r)_{basal}^{(n)} \quad (5)$$

with $n = 1, 2, \dots, 50$. Processing is stopped when $\max|\hat{I}(r)_{basal}^{(n)}| < 1$ cm. Once the image has been preprocessed, we perform the segmentation in two blocks. The first is the segmentation level image based on filtering in the frequency domain and binarization by threshold; the second is a level surface that is basically an analysis by level sets.

3.3. Segmentation using 2D discrete Fourier transform

In this section we describe the segmentation algorithm at image level, in which any pixel segmented is not rated. The algorithm is based on the discrete Fourier transform. First the 2D discrete Fourier Transform $\tilde{I}(\omega) = \mathcal{F}\{\tilde{I}(r)\}$ is applied to the depth image $\tilde{I}(r)$. To filter, the data is shifted to center the spectrum and then processed using a Gaussian low pass filter $\tilde{I}_f(\omega) = \tilde{I}(\omega)G(\omega)$.



Kolmogorov-Smirnov Test		
D_n	0.122	
α	0.05	
$D_n < C_{n,\alpha} \sqrt{\frac{n_1+n_2}{n_1*n_2}}$	0.12 < 0.16	
Statistical parameters	Manual ϕ	Kinect ϕ
Mean	-5.369	-5.613
Std dev	1.166	1.130
Skewness	0.160	0.260
Kurtosis	0.960	1.140

Fig. 10. Results obtained from Area 2, Quaternary conglomerate. (A) Color image; (B) depth image; (C) shows ECDF resulting from manual analysis and automatic method, the maximum difference is 12.2%; and (D) Kolmogorov-Smirnov test and statistical parameters. (For interpretation of the references to color in this figure legend, the reader is referred to the web version of this article.)

The cutoff frequency is a parameter that must be set manually so that the best frequency response is obtained. The inverse Fourier transform $\hat{I}_f(r) = \mathcal{F}^{-1}\{I_f(\omega)\}$ is applied to the filtered image to better define the contours of the depth image in the spatial domain. Fig. 3 shows an example of a filtered sample area. The image is then convolved with a 5×5 Gaussian Laplacian filter (LoG) with $\sigma = 0.05$. The filter is expressed mathematically as

$$\nabla^2 G(p) = -\frac{1}{2\pi\sigma^2} \left(2 - \frac{x^2 + y^2}{\sigma^2} \right) \exp\left(-\frac{x^2 + y^2}{2\sigma^2}\right). \quad (6)$$

Finally the image is binarized with a threshold of 0.05, with 0 being black and 1 white. For contours and area of the clast functions, the MATLAB[®] morphological operations “clean,” “spur pixels,” “thin” and “traces the exterior boundaries of objects” are used.

3.4. Segmentation using level sets

Another section of the block is a segmentation algorithm based on level sets. As mentioned above, the depth image can be seen as a topographic map or digital elevation model. A method commonly employed in topographic maps is contour lines by isoelevation; namely drawing contour lines that are at the same height. The level set can be represented as a plane with an isovalue. Fig. 4

illustrates an example of a plane with different level sets. In each isovalue plane, we obtain a contour of each clast. The level which we consider the boundary is closest to the real clast edges and is the lowest before intersecting with another contour. We observed that the contours are closer to the edges if we use planes with angles. The planes are generated by directional cosines, but for now the angles that give the best response were chosen manually. In Fig. 5 the intersection of the deposit area with an inclined plane is shown. If in plane $P(r, \phi)$ we obtain a contour c_m^ϕ which is the approximation to the clast edges m of the plane in terms of angle ϕ , then m clast edges are the intersections of the contours of each plane. This may be defined as

$$C_m = c_m^{\phi_1} \cup c_m^{\phi_2} \cup \dots \cup c_m^{\phi_n} \quad (7)$$

where C_m is the approximation of the edges and n is the number of angles used. Pseudocode 1 best describes the segmentation by contour lines.

3.4.1. Pseudocode 1

The mask for the count is the union of the blocks resulting from the segmentation, Fourier and level sets. To apply the Rosiwal intercept method, a binary image of the same size as the depth with a horizontal line series is created. The spacing between the lines is chosen so that the same particle is intersected no more than twice

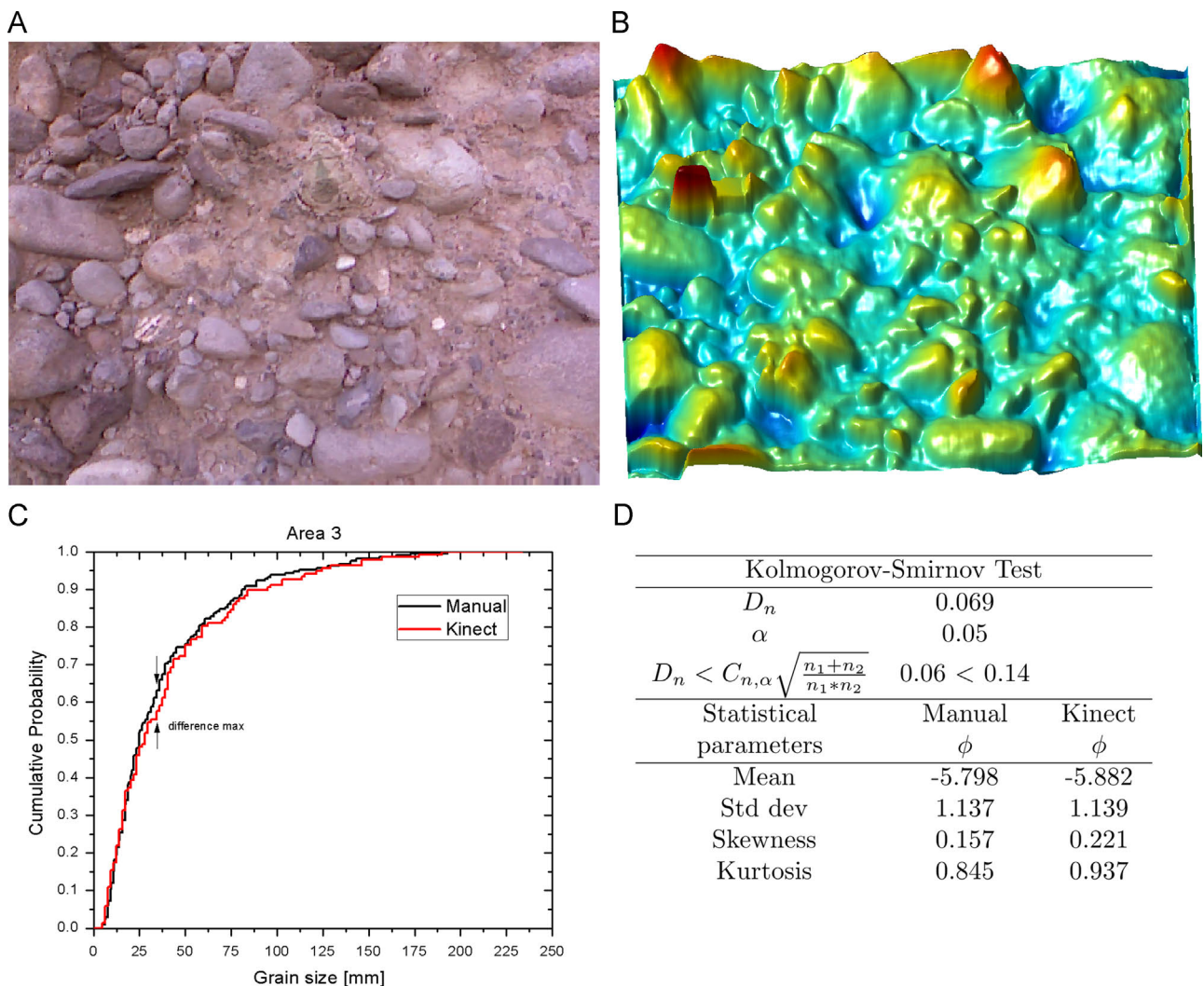


Fig. 11. Results obtained from Area 3, Quaternary conglomerate. (A) Color image; (B) depth image; (C) graph of ECDF resulting from manual analysis and the new system developed here, with a maximum difference of 6.9%; and (D) Kolmogorov–Smirnov test and statistical parameters. (For interpretation of the references to color in this figure legend, the reader is referred to the web version of this article.)

after the intersections between the grid lines and the mask have been found by logical operations. The spatial calibration of intersections is obtained from the relation between the FOV angles and depth.

4. Results and discussion

4.1. System performance

In the following section we show the results of the implementation of the proposed system in eight outcrop areas with favorable environmental conditions. The distance between the Kinect and the outcrop depends on accessibility and the area we set out to cover. The Kinect–wall distance ranged from 85 to 103 cm, corresponding to areas between 0.68 and 1.06 m². The distances and areas of each shot are listed in Table 2. The quantization level was calculated by Eq. (1) given above in the Kinect device section. The lowest was 2 mm and the highest was 3 mm; this serves as a reference because when working in the field with adverse lighting conditions, the resolution tends to be lower. In addition to the depth image, a color image (RGB) was captured in order to make the comparison between the proposed method and the manual optical method.

The eight depth images presented noise probably caused by corners, the type of material or lighting conditions. The effect of these factors was significantly reduced by the pre-processing stage. The first noise reduction strategy consists in setting all pixels with value greater than three times the average height equal to zero. This can best be described with reference to Fig. 6, where (B) and (C) show the depth image and its first preprocessing, respectively, and (D) shows the smoothed image resulting from applying the Gaussian kernel filter. Once the image has been filtered, the basal surface is calculated.

Because the Fourier-based segmentation method is supervised, we need to manually define the matrix covariance associated with the Gaussian filter, so in the analyzed images the variance is equal in x and y. For this reason they were set to 10, 12, 15, 20, 12, 8, 9 and 13 for Areas 1 to 8 respectively. In all cases $\sigma = 0.05$ for the LoG filter and the threshold for binarizing the image was the same; i.e. 0.05. Because the segmentation stage is performed at image level, the edges found do not correspond in some cases to the real clast edges; rather they represent clast roughness and this can result in oversegmentation, which is illustrated in Fig. 7 in which the result from Area 4 is shown.

In the segmentation stage based on level sets, each depth image was processed by four planes; one at 0°, another with an

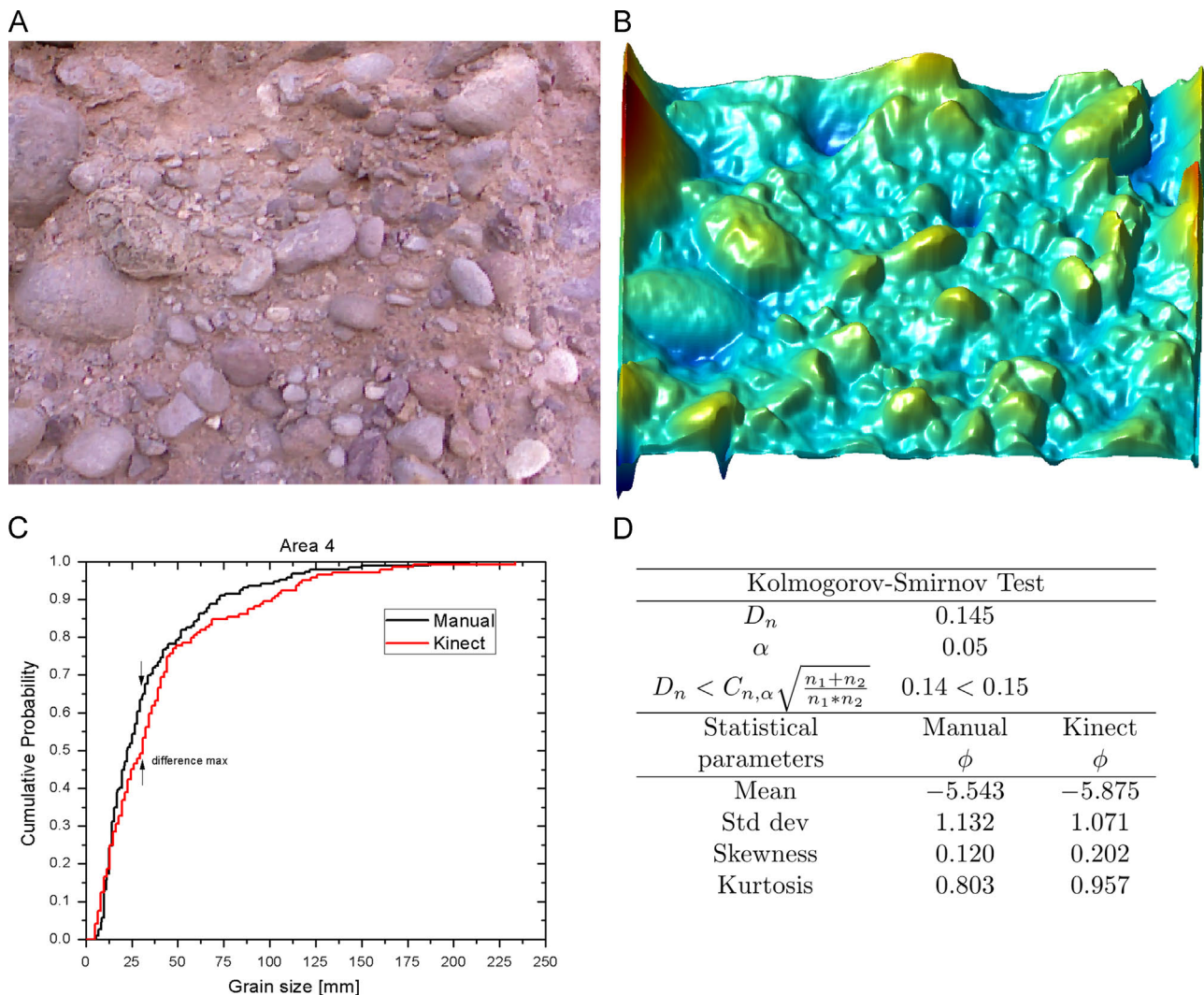


Fig. 12. Results obtained from Area 4, Quaternary conglomerate. (A) Color image; (B) depth image; (C) graph of ECDF resulting from manual analysis and the new system developed here, obtaining a maximum difference of 14.5%; and (D) Kolmogorov–Smirnov test and statistical parameters. (For interpretation of the references to color in this figure legend, the reader is referred to the web version of this article.)

angle such that the maximum value of the plane is equal to the average height of the depth image, and the other two angles, 0.7° and 2.0° , were proposed manually based on the clast heights. The contour of the mask resulting from the segmentation of Area 1 (Fig. 8) shows continuity and presents no oversegmentation. In Fig. 8 the segmentation contour resulting from the union of the masks obtained by the two segmentation stages is shown in green.

After the masks resulting from the two previous segmentation stages were obtained, the Rosin-Rammler stereological method was applied. A binary image is created with a horizontal grid, each line having a defined distance such that a clast is not crossed by more than two lines. In order to find the intersections between the grid lines and the clasts, we use the logical “AND” operation. The image calibration is calculated from the ratio between the FOV, the distance between the Kinect device and the outcrop, and image size. For purposes of comparison, the grid lines and calibration were the same for the proposed automatic system and the manual analysis. For every area of the outcrop we used a depth image (16 bit and size 480×640 pixel) for the automatic analysis and a color image (RGB) for the manual optical analysis. In Figs. 9–16 (A and B), the analyzed color and depth images are shown.

The grain size distributions analyzed in this study include clasts from -2ϕ to -7ϕ (4 mm to 256 mm). The automatic and manual

analyses were compared using the empirical cumulative distribution function (ECDF). The maximum differences between automatic and manual distribution functions of the analyzed areas were between 7% and 14% in the range of -2ϕ to -5ϕ (Figs. 9–16C). Fewer clasts were found by the proposed automatic method than by the manual one, with differences ranging from 10 to 45%. With these features, the non-parametric Kolmogorov–Smirnov test demonstrates that there is a 0.95 probability that the two ECDF have the same behavior in six of the outcrop areas (Areas 1 to 5 and Area 8) and there is a 0.90 probability for Areas 6 and 7. Statistical parameters of size distribution normally used in granulometric and sedimentological studies such as the mean and standard deviation were compared for the manual and automatic analysis, and a high similarity in the distribution shapes was found. The skewness parameter has the same sign for both methods except for Area 7, where the automatic method provides a tendency towards the coarse fraction. In the alluvial outcrop (Area 6), a clear tendency towards the finer fractions was observed. The kurtosis parameter showed similar trends for the two methods.

Based on the results of the statistical parameters and the Kolmogorov–Smirnov test, it has been validated that the granulometries obtained using the Kinect device have a high probability of having the same characteristics as those obtained manually, and it has also been

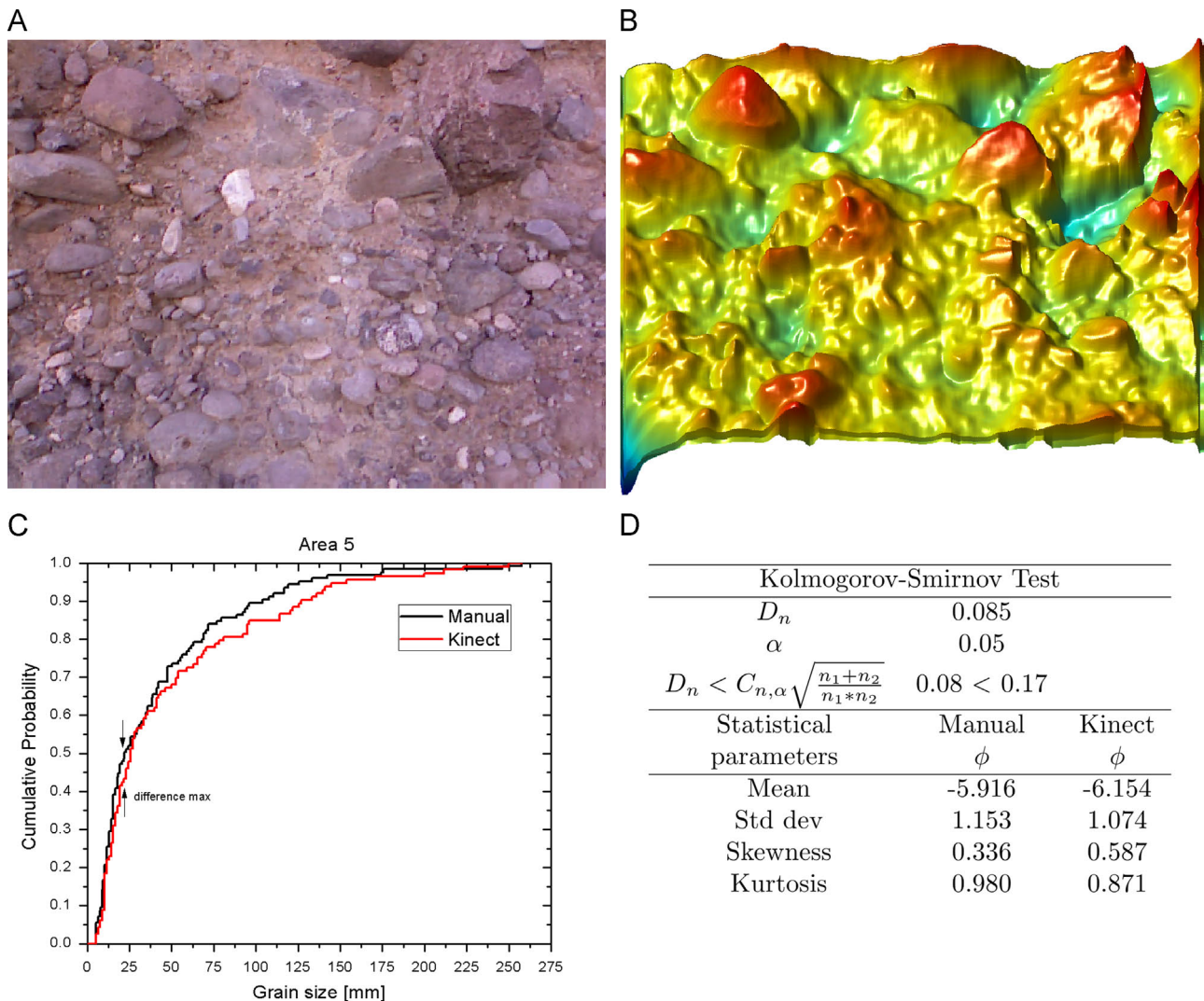


Fig. 13. Results obtained from Area 5, Quaternary conglomerate. (A) Color image; (B) depth image; (C) graph of ECDF resulting from manual analysis and the new system developed here, the maximum difference is 8.5%; and (D) Kolmogorov–Smirnov test and statistical parameters. (For interpretation of the references to color in this figure legend, the reader is referred to the web version of this article.)

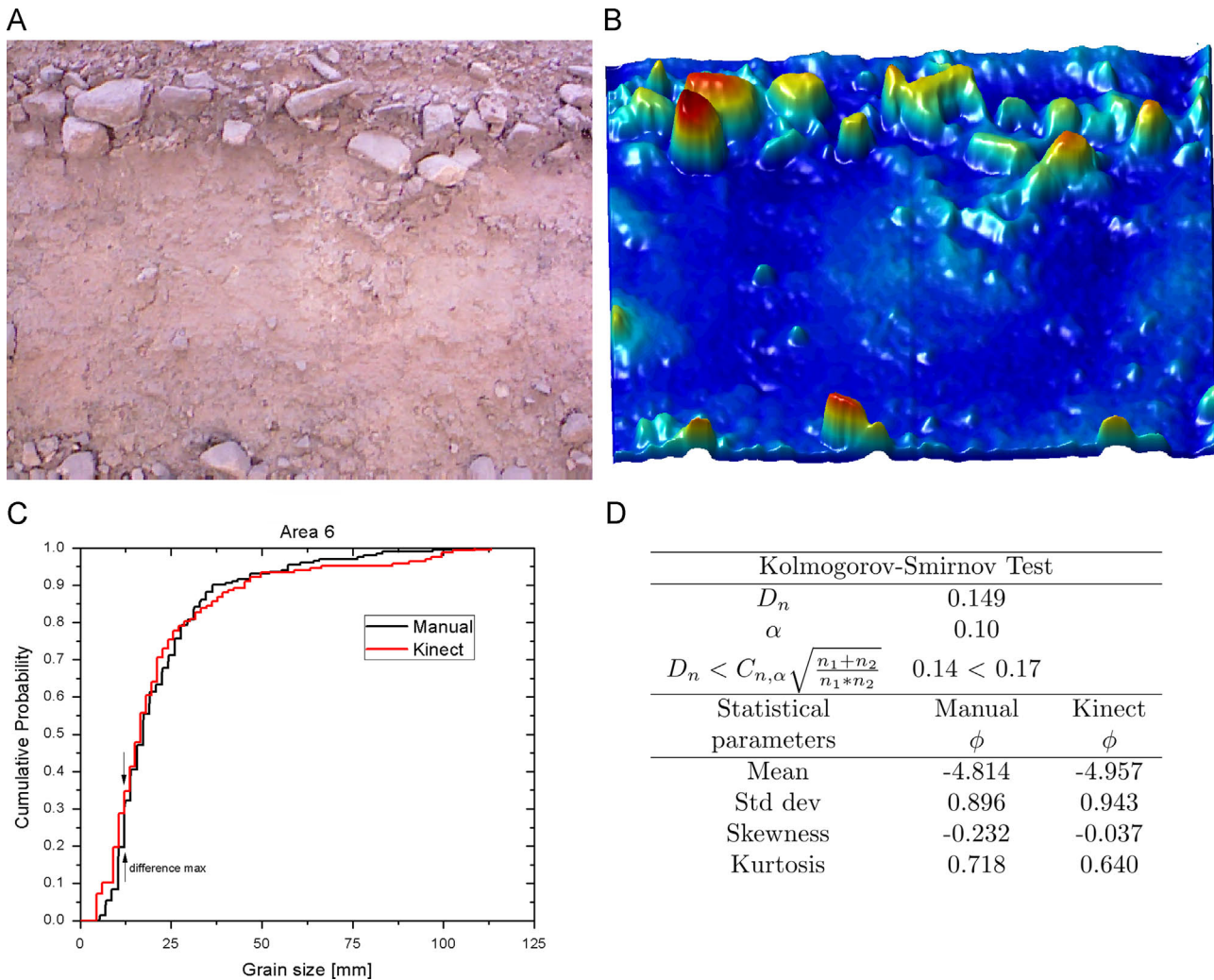


Fig. 14. Results obtained from Area 6, alluvial deposit. (A) Color image; (B) depth image; (C) graph of ECDF resulting from manual analysis and the new system developed here, the maximum difference between them is 14.9%; and (D) Kolmogorov–Smirnov test and statistical parameters. (For interpretation of the references to color in this figure legend, the reader is referred to the web version of this article.)

proved that the proposed system provides completely repeatable data, a property that is not possessed by the classical methods of sieving and manual optical analysis. The average difference between the ECDF on the eight outcrops was 11%. This variation could be due to the manual counting method, which strongly depends on human operator performance. Regardless of this fact, six of the eight total areas had a probability of 0.95 that CDFs obtained by both methods showing the same behavior. This leads us to suggest that the system represents a cutting-edge methodology for automatic granulometric analysis and it is completely feasible to replace the manual method by this new method. An important advantage is that despite being a supervised algorithm, it can analyze multiple areas without being difficult for users.

Another important characteristic of this system is that it can obtain the granulometry from a tridimensional digital model. This gives it many advantages over other optical methods, because segmentation is performed based on the volume of the clasts, so that the only characteristic that must be considered in order to have good measurements is that the clasts must have a clear volumetric difference from the matrix. This makes the method more robust than others that use only color or texture segmentation, because most natural outcrops show a wide range of textures and colors, which makes it difficult to apply one single segmentation algorithm on different outcrops. Moreover, using the Kinect

device for capturing the DEM makes this system easy to transport. The device works flawlessly on a laptop computer, with good resolution depth of images in small areas, and it can capture quite large areas in just a few milliseconds. In addition, the cost of this device is very much less than that of professional granulometric devices. The capture, processing and analysis algorithms were given a user-friendly graphic interface (GUI) developed in MATLAB. This interface has basic controls of the number of frames and angle, resulting in perfect visualization of the color and depth image. The segmentation GUI allows all the variables of the Fourier analysis and contour lines to be controlled (see Section 3) which enables visualization of the mask resulting from segmentation. Lastly, the Rosiwal stereological method control box allows image rotation, changing space between lines, calibration and visualization, and finally exporting the results to an Excel file. The software is freely available at http://www.laima-uaslp.org/kinect_soft.html.

4.2. Limits of the method

Despite the good performance demonstrated by the method, there are still some methodological limitations (Table 3). One of the most important, which directly affects the resolution of the system, is the illumination: the Kinect device works only under certain illumination conditions. For this paper we used the system

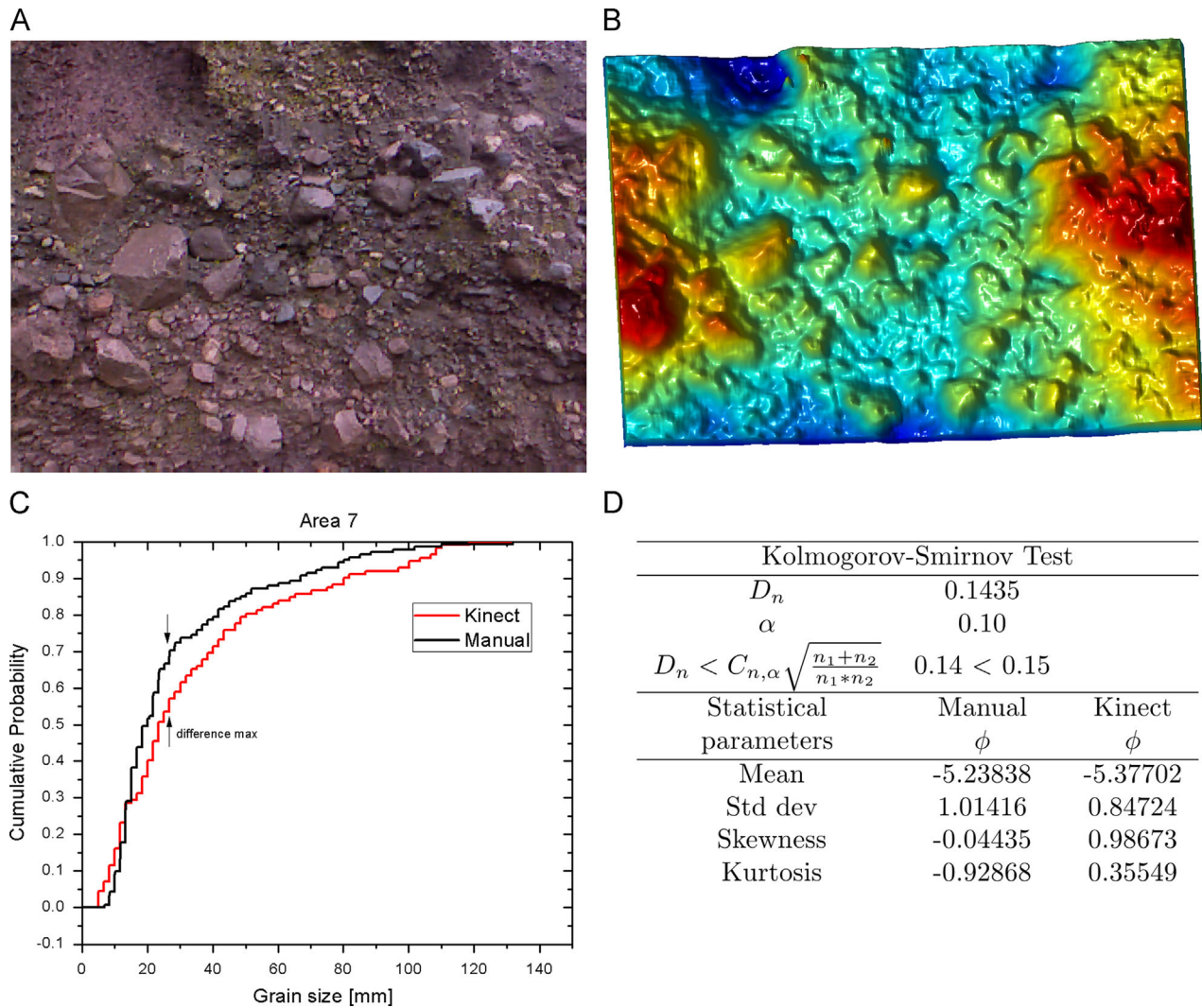


Fig. 15. Results obtained from Area 7, debris flows. (A) Color image; (B) depth image; (C) graph of ECDF resulting from manual analysis and the new system developed here, the maximum difference between them is 14.3%; and (D) Kolmogorov–Smirnov test and statistical parameters. (For interpretation of the references to color in this figure legend, the reader is referred to the web version of this article.)

in the field but it was impossible to get any data when the sunlight shone directly on the outcrop or the Kinect device. For outdoor applications it will operate accurately only at certain hours of the day when light is soft (morning or afternoon, or cloudy days), or in semi-controlled illumination conditions (using a tarp to prevent direct light). Another limitation is the inverse relation between resolution and area; the higher the resolution, the smaller the area and vice versa. In order to solve this problem we will propose further work in which we will provide software by which depth images can be stitched together. This procedure will enable larger areas to be captured with higher resolution, resulting in smaller statistical error.

The outcrop's structural and textural characteristics are essential aspects to consider before performing a deposit analysis using this device. In order to carry out a satisfactory analysis it is very important that the clasts "stick out" from the outcrop wall. This implies that the deposit matrix should preferably be soft or unconsolidated so that clast outlines will have been enhanced by erosion. The outcrop surface inside the area of interest must be quite regular. Particle size is also important for accurate results. When particles are smaller than 4 mm or bigger than 256 mm (this problem will be solved when we have the ability to analyze larger areas by stitching together the basic area units as used in this paper) the resulting measures could be out of the reliable

range and could introduce errors due to the resolution of the Kinect device. A problem that could rise with very irregular blocks is that the algorithm could confuse surface irregularities of a single clast with multiple clasts.

Another characteristic to take into account is the accessibility of an outcrop. Because the optimal range of the instrument is 0.8 to 1.0 m (although useful measures can still be obtained at 3.5 m) and the angle between the sensor and the analyzed surface is limited to few degrees around 90°, obtaining an appropriate geometric setup for image acquisition may not be trivial. Shooting images from less than optimal positions can produce discontinuities or holes in the depth map, usually at the edges of objects (Nguyen et al., 2012). In order to obtain good measures, the outcrop must be also free of vegetation and fine particles sticking to the surface.

5. Conclusion

The new system proposed here enables grain size distributions in sedimentary deposits to be measured over a large range of clast sizes from pebbles to blocks. The innovative content of this work is important for many reasons. It uses a very low cost device widely available in the market: the Microsoft Kinect. A special segmentation technique developed for the three-dimensional model by

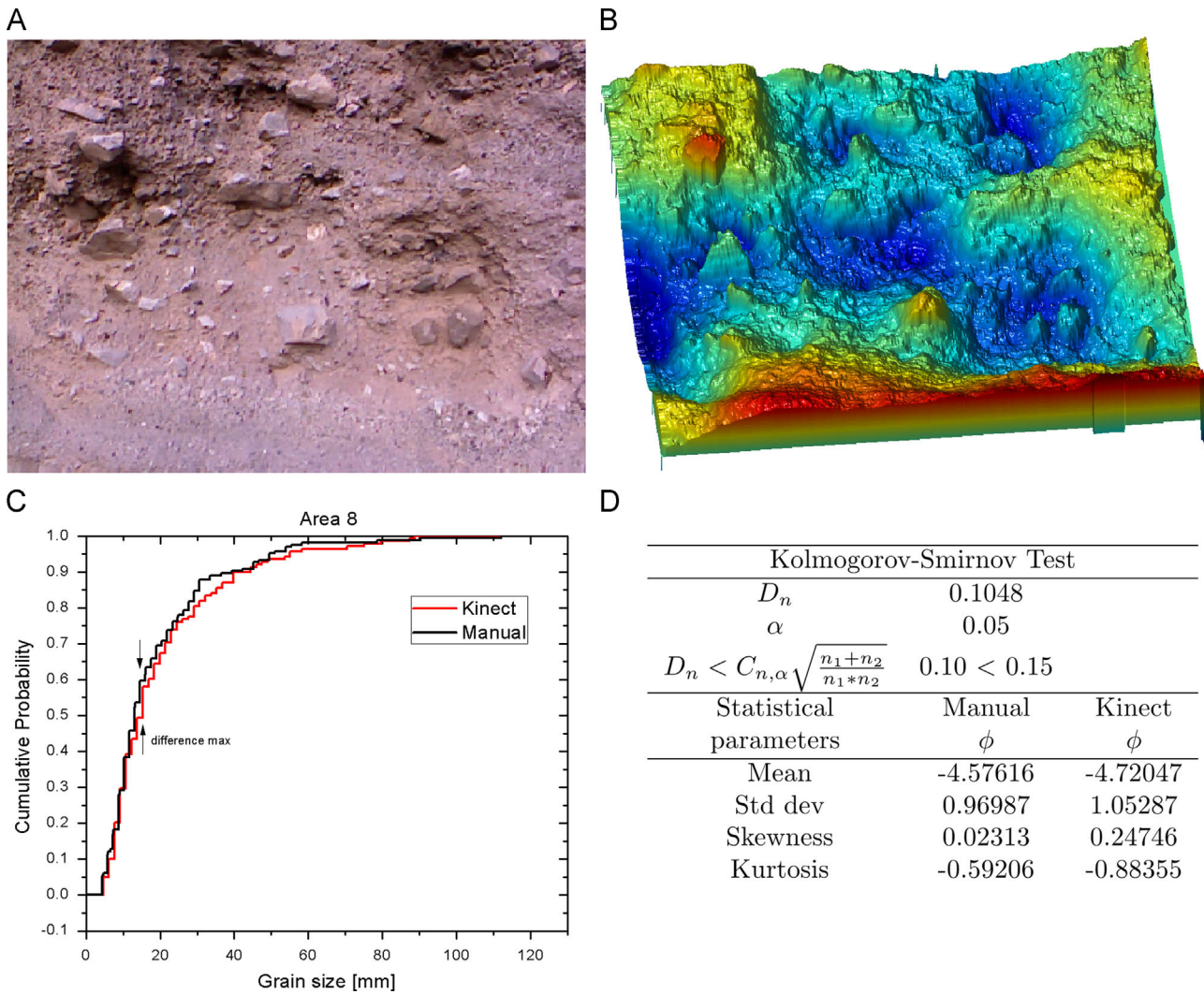


Fig. 16. Results obtained from Area 8, pyroclastic deposit. (A) Color image; (B) depth image; (C) graph of ECDF resulting from manual analysis and the new system developed here, the maximum difference is 10.4%; and (D) Kolmogorov–Smirnov test and statistical parameters. (For interpretation of the references to color in this figure legend, the reader is referred to the web version of this article.)

Table 3
Limitations and possible solutions for some common methodological problems.

Condition	Example	Possible solution
Excessive lighting Planar wall of the outcrop	Clear day, direct sun on the outcrops Ignimbrite outcrops in quarries	Using a tarp to shade the area of analysis Washing the outcrop surface when matrix is soft. No solution for hardened deposits cut by machines
No clasts bigger than 4 mm	Surge deposits, fine sedimentary deposit	No solution
Individual clasts with an area greater than the 25% of the visual field of the Kinect	Avalanche deposits, block and ash flows, debris flows	Increasing the distance between the wall and the Kinect expands the visual field. An alternative solution is stitching together several basic Kinect areas by a specific software (freely available soon from the authors)
Outcrop inaccessible	Presence of obstacles, rivers, vegetation, steep slope	Search for an equivalent area of the deposit with better accessibility conditions
Presence of clasts with translucency or diffuse reflection properties	Obsidian-rich lava flows	No solution
Blocks with very irregular surface	Might appear in debris avalanche, pyroclastic flows and debris flow deposits	Avoid measuring areas with this kind of clast outcropping

Pseudocode 1

Pseudocode 1: Segmentation using level sets

Input variables

$\tilde{I}(r) \leftarrow$ Image depth

$\Phi(\phi_1, \phi_2, \dots, \phi_n) \leftarrow$ Angles of the planes

$\tilde{I}_p(r_p, \Phi) \leftarrow$ Isoplane

Table 3 (continued)

Condition	Example	Possible solution
Contour analysis begins		
for $n=1$ to number of angles//planes loop		
$p(\Phi(n)) =$ plane with angle ϕ_n		
$L =$ from max of p is equal to min of the $\hat{I}(r)$ to min of p is equal to max of the $\hat{I}(r)$		
for $ls=1$ to length (L)//levels set loop		
$m =$ clasts found		
$c(p, L(ls), m(i)) =$ contour of the i clast in the $L(ls)$ level of p plane		
End		
$C(p, m) =$ lowest contours of the clasts before intersects with another		
End		
segmented image = intersection of the $C(p(\Phi), m)$ contours found in all planes		
Contour analysis ends		

means of custom software is available to the scientific community as freeware. The new methodology demonstrates proven reliability compared with other well-known methodologies commonly used in sedimentology. Through comparison of the ECDFs by the Kolmogorov–Smirnov test it has been proven that the system has a high probability of producing distributions that have the same behavior as those produced by a manual counting analysis. The use of the Kinect and processing by means of the graphic interfaces developed here make this a low-cost tool that makes it easier to obtain grain size distributions. At the present time, due to resolution limits of the images captured by the device, it is not suitable for clasts with a diameter smaller than -2ϕ . But new technological development in devices of this type, perhaps not limited only to the Kinect, will enable the minimum size of clasts that can be detected to be reduced in the future. We believe that this new analysis, segmentation and grain size discrimination methodology will be able to be implemented with minimal modifications, if any, in future devices that offer better image resolution and other improved technology.

Besides the limitations related to the Kinect device there are some characteristics that the outcrop must have in order to obtain an accurate analysis, such as the relief, type of materials and accessibility. However, in this paper we propose a series of possible solutions to these methodological limitations.

We believe that this new methodology is a useful tool for sedimentology and earth science studies, as it enables fast grain size distribution measurement in deposits where a rapid and reliable practical size distribution is required, as well as the potential to obtain granulometric measurements and their spatial variability in the outcrop (2D granulometric maps).

The software is available to the scientific community as a full freeware product which can be downloaded from the LAIMA laboratory site: http://www.laima-uaslp.org/kinect_soft.html.

Acknowledgements

We wish to thank Anibal Montenegro Ríos for support during the experimental work and for useful discussions. We also are grateful to Margaret Schroeder Urrutia for her observations about the English. We also thank Instituto de Geología and Facultad de Ciencias of UASLP.

This work was partially supported by Ciencias Básica CONACYT projects SEP-83301, SEP 184060 and SEP 168140, PROMEP UASLP-

PTC-241 Project funds. GMC and LARS acknowledge CONACYT for grants no. 229958 and no. 303315.

References

- Allan, T., 2003. first ed. *Powder Sampling and Particle Size Determination*, vol. 1. Elsevier Science, Amsterdam p. 682.
- Bunte, K., Abt. S. R., 2001. Sampling Surface and Subsurface Particle-size Distributions in Wadable gravel- and Cobble-bed Streams for Analyses in Sediment Transport, Hydraulics, and Streambed Monitoring, Dept. of Agriculture, Forest Service, U.S., 428 pp.
- Chayes, F., 1956. *Petrographic Modal Analysis: An Elementary Statistical Appraisal*. Wiley, New York p. 113.
- Cruz, L., Lucio, D., Velho, L. Kinect and RGBD images: challenges & applications. In: 25th SIBGRAPI Conference on Graphics, Patterns and Images Tutorials (SIBGRAPI-T) 2012, 22–25 Aug. 2012 2012, pp. 36–49.
- Essmaeel, K., Gallo, L., Damiani, E., De Pietro, G., Dipanda, A. Temporal denoising of Kinect depth data. In: Eighth International Conference on Signal Image Technology and Internet Based Systems (SITIS) 2012, 25–29 Nov. 2012, pp. 47–52.
- Islam, M. R., Rahaman, S., Hasan, R., Noel, R. R., Salekin, A., Ferdous, H. S. 2013. A novel approach for constructing emulator for Microsoft Kinect XBOX 360 sensor in the NET platform. In: Fourth International Conference on Intelligent Systems Modelling & Simulation (ISMS), 2013, 29–31 Jan. 2013, pp. 1–6.
- Jingjing, F., Wang, S., Yan, L., Shipeng, L., Wenjun, Z., 2012. Kinect-like depth denoising, circuits and system (ISCAS). In: 2012 IEEE International Symposium, 20–23 May 2012, pp. 512–515.
- Jungong, H., Ling, S., Dong, X., Shotton, J., 2013. Enhanced computer vision with Microsoft Kinect sensor: a review. *IEEE Trans. Cybern.* 43 (5), 1318–1334, <http://dx.doi.org/10.1109/tycb.2013.2265378>.
- Jutzeler, M., Proussevitch, A.A., Allen, S.R., 2012. Grain-size distribution of volcanoclastic rocks 1: a new technique based on functional stereology. *J. Volcanol. Geotherm. Res.* 239–240, pp11–11.
- Khoshelham, K., Elberink, S.O., 2012. Accuracy and resolution of Kinect depth data for indoor mapping applications. *Sensors* 12, 1437–1454.
- Lewis, D.W., McConchie, D., 1994. *Analytical Sedimentology*. Chapman & Hall, New York, London p. 197.
- Liyong, C., Qi, S., Han, S., Yang, C., Shuying, Z., 2012. Design and implementation of human-robot interactive demonstration system based on Kinect. In: Control and Decision Conference (CCDC) 2012 24th Chinese, 23–25 May 2012 pp. 971–975.
- Lovell, C.J., Rose, C.W., 1991. Wake-capture effects observed in a comparison of methods to measure particle settling velocity beyond Stokes' range. *J. Sediment. Petrol.* 61, 575–582.
- Mankoff, K.D., Russo, T.A., 2012. The Kinect: a low-cost, high-resolution, short-range 3D camera. *Earth Surf. Processes Landforms*.
- Mouton P. R., 2002. *Principles and Practices of Unbiased Stereology: An Introduction for Bioscientists*. Baltimore, London, 232 pp.
- Nguyen, C. V., Izadi, S., Lovell, D. Modeling Kinect sensor noise for improved 3D reconstruction and tracking. In: 3D Imaging, Modeling, Processing, Visualization and Transmission (3DIMPVT) 2012 Second International Conference on, 13–15 Oct. 2012 pp. 524–530.
- Olgun, E., Norman, T., 1993. Grain size analysis of some olistostromes between alkuyumcu and Alci (SW Ankara). *Bull. Mineral Res. Explorat.* 115, 31–48. OpenKinect. (<http://openkinect.org/>) [Online]. [Accessed 6th June 2013].

- OpenNI. (<http://www.openni.org/>) [Online]. [Accessed 19th June 2013].
- Roverato, M., Capra, L., Sulpizio, R., Norini, G., 2011. Stratigraphic reconstruction of two debris avalanche deposits at Colima Volcano (Mexico): insights into pre-failure conditions and climate influence. *J. Volcanol. Geotherm. Res.* 207 (1–2), 33–46.
- Sahagian, D.L., Proussevitch, A.A., 1998. 3D particle size distributions from 2D observations: stereology for natural applications. *J. Volcanol. Geotherm. Res.*, 173–196.
- Sarocchi, D., Borselli, L., Macías, J.L., 2005. Construcción de perfiles granulométricos de depósitos piroclásticos por métodos ópticos. *Revista Mexicana de Ciencias Geológicas* 23 (2), 371–382.
- Sarocchi, D., Sulpizio, R., Macías, J.L., Saucedo, R., 2011. The 17 July 1999 block-and-ash flow (BAF) at Colima Volcano: New insights on volcanic granular flows from textural analysis. *J. Volcanol. Geotherm. Res.* 204, 40–56.
- Saucedo, R., Macías, J.L., Sarocchi, D., Bursik, M., Rupp, B., 2008. The rain-triggered Atenquique volcanoclastic debris flow of October 16, 1955 at Nevado de Colima Volcano, Mexico. *J. Volcanol. Geotherm. Res.* 173 (1–2), 69–83.
- Smisek, J., Jancosek, M., Pajdla, T. 2011. 3D with Kinect. In: IEEE International Conference on Computer Vision Workshops (ICCV Workshops), 2011, 6–13 Nov. 2011, pp. 1154–1160.
- Stein, R., 1985. Rapid grain-size analyses of clay and silt fraction by SediGraph 5000D; comparison with Coulter counter and Atterberg methods. *J. Sediment. Petrol.* 55, 590–593.
- Syvitski, James P.M., 1991. Principles, Methods and Application of Particle Size Analysis, first ed. Cambridge University Press, Cambridge.
- Windows, Kinect for Windows (<http://www.microsoft.com/en-us/kinectforwindows/>) [Online]. [Accessed 19th June 2013].
- Zhengyou, Z., 2012. Microsoft Kinect sensor and its effect. *IEEE MultiMedia* 2, 4–10.